REFERENCES

[1] E. F. Schlömann, "Microwave behavior of partially magnetized ferrites," *J. Appl. Phys.*, vol. 41, no. 1, Jan. 1970.

[2] K. S. Yee, "Numerical solution of initial boundary value problems involving Maxwell's equations in isotropic media," *IEEE Trans. Antennas Propagat.*, vol. AP-14, pp. 302–307, May 1966.

[3] A. Reineix, T. Monediere, and F. Jecko, "Ferrite analysis using the finite-difference time-domain (FDTD) method," *Microwave Opt. Tech. Lett.*, vol. 5, pp. 685–686, Dec. 1992.

[4] J. A. Pereda, L. A. Vielva, A. Vegas, and A. Prieto, "A treatment of magnetized ferrites using the FDTD method," *IEEE Microwave Guided Wave Lett.*, vol. 3, pp. 136–138, May 1993.

[5] ____, "FDTD analysis of magnetized ferrites: Approach based on the rotated Richtmyer difference scheme," *IEEE Microwave Guided Wave Lett.*, vol. 3, pp. 322–324, Sept. 1993.

[6] J. A. Pereda, L. A. Vielva, M. A. Solano, A. Vegas, and A. Prieto, "FDTD analysis of magnetized ferrites: Application to the calculation of dispersion characteristics of ferrites loaded waveguides," *IEEE Trans. Microwave Theory Tech.*, vol. 43, pp. 350–357, Feb. 1995.

[7] L. A. Vielva, J. A. Pereda, A. Vegas, and A. Prieto, "Calculation of scattering parameters of ferrite-loaded waveguides using the FDTD method," in *23rd European Microwave Conf.*, Madrid, Spain, Sept. 1993, pp. 285–287.

[8] J. A. Pereda, L. A. Vielva, A. Vegas, and A. Prieto, "An extended FDTD method for the treatment of partially magnetized ferrites," *IEEE Trans. Magn.*, vol. 31, pp. 1666–1669, May 1995.

[9] C. Melon, Ph. Leveque, T. Monediere, A. Reineix, and F. Jecko, "Frequency dependent finite-difference time-domain (FDTD) formulation applied to ferrite material," *Microwave Opt. Tech. Lett.*, vol. 7, no. 12, Aug. 1994.

[10] B. Engquist and A. Majda, "Absorbing boundary conditions for the numerical simulation of waves," *Math. Comput.*, vol. 31, pp. 629–651, 1977.

[11] K. Berthou-Pichavant and Ph. Gelin, "Wave propagation in non saturated ferrites: Use in modeling," in *Int. Symp. Non Linear Electromag. Syst.*, F35, Cardiff, U.K., Sept. 1995.

HBT's RF Noise Parameter Determination by Means of an Efficient Method Based on Noise Analysis of Linear Amplifier Networks

Philippe Rouquette, Daniel Gasquet, Tony Holden, and Jonathan Moult

***Abstract*— A method for the evaluation of the RF noise figure of heterojunction bipolar transistors (HBT's) is presented. The noise analysis is based on the use of the correlation matrices. The two-port device is described as an interconnection of basic two-port devices whose noise behavior is known. The circuit theory of linear noisy networks shows that any two-port device can be replaced by a noise equivalent circuit which consists of the original two-port assumed to be noiseless and possess two additional noise sources. The purpose of this paper is to obtain the four noise parameters of the device, taking into account the access resistances and inductances. The calculations presented show good agreement with measurements, and as a consequence, they permit a good estimation of the noise performance of the structure without neglecting any parasitic elements of the equivalent circuit.**

I. INTRODUCTION

Heterojunction bipolar transistors (HBT's) have recently demonstrated improved RF performances into microwave frequencies with the advent of self-aligned technologies and innovative isolation approaches to reduce parasitic effects. Therefore, it becomes important to analyze the exact causes of device limitations in terms of the HBT's equivalent circuit representation [1]–[3] and noise behavior. In Section II of this paper, the different details of the direct calculation of the HBT's T-like small signal equivalent circuit extracted from S-parameter measurements is presented. Noise analysis [4] is then presented in Section III, starting from the intrinsic impedance representation in order to calculate the noise of the total extrinsic transistor. Finally, in Section III, comparisons are presented between calculations and measurements.

II. FORMALISM FOR DIRECT EXTRACTION OF HBT'S EQUIVALENT CIRCUIT PARAMETERS

The GaInP/GaAs HBT's characterized in this work were fabricated by GEC Marconi. The authors have investigated single finger devices with effective emitter area of $3 \times 12 \ \mu m^2$ (J_1) and $3 \times 20 \ \mu m^2$ (J_2). The metal–organic chemical vapor deposition (MOCVD) grown device-layer structure consists of a 2800-Å GaAs emitter cap n^+-doped ($4 \times 10^{18}/cm^3$), two GaInP emitter layers of 200 Å n^+-doped ($2 \times 10^{18}/cm^3$) and of 1000 Å n-doped ($3 \times 10^{17}/cm^3$), 1000 Å GaAs base layer p^{++}-doped ($3 \times 10^{19}/cm^3$), 0.5-μm GaAs pre-collector n^--layer doped ($10^{16}/cm^3$) and 0.7-μm GaAs collector n^+-doped ($2 \times 10^{18}/cm^3$), all grown on a semi-insulating substrate.

The HBT's equivalent circuit used for this paper is the conventionally accepted T model [5]. This circuit is divided in three parts: the intrinsic part, the part in which the feedback capacitance is taken into account, and the extrinsic part (each of them represented by the matrix $[Z]_i$, $[Y]_j$, and $[Z]_k$), respectively. Scattering parameters have been measured for different bias points with an HP8720B network

Manuscript received March 18, 1996; revised January 24, 1997.

P. Rouquette and D. Gasquet are with the Centre d'Electronique de Montpellier, Université Montpellier II, F-34095 Montpellier cedex 05, France.

A. Holden and J. Moult are with GEC Marconi, Caswell Towcester Northands, NN 12 8EQ, U.K.

Publisher Item Identifier S 0018-9480(97)02905-0.

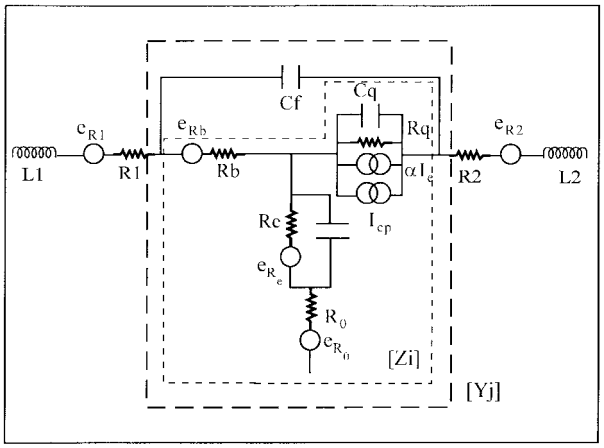

Fig. 1. Noisy T-like topology small-signal equivalent circuit including thermal- and shot-noise generators.

analyzer under a probe station from 200 MHz to 18 GHz. The circuit model (Fig. 1) includes extrinsic parasitic elements R_1, L_1, R_2, and L_2 which represent the access and contact resistances, and inductances of the access lines. Thus, they are bias independent. To obtain these elements, the transistor S-parameters are measured in their nonconducting state ($I_b = 0\ \mu$A, $V_{be} = 0$ V). As a consequence, the resulting expressions are simpler ($\alpha = 0$, $R_E = \infty$). Access resistances and inductances are extracted from the following extrinsic matrix expressions:

$$[Z_{11} - Z_{12}]_k = \Re_1 + j\Im_1 \tag{1}$$

$$[Z_{22} - Z_{21}]_k = \Re_2 + j\Im_2 \tag{2}$$

where it is as shown in (3)–(6) at the bottom of the following page. For frequencies higher than 6 GHz $\Re_1$ and $\Re_2$ are frequency independent and $\Im_1$ and $\Im_2$ are linear as a function of frequency. Thus, one can easily deduce $\Re_1 \approx R_1$, $\Im_1 \approx L_1\omega$, $\Re_2 \approx R_2$, and $\Im_2 \approx L_2\omega$.

Once one obtains these four access elements, one subtracts them from the extrinsic matrix $[Z]_k$ in order to calculate the $[Y]_j$ admittance matrix, and as a consequence, the feedback capacitance C_F as

$$[Z]_j = [Z]_K - \begin{bmatrix} R_1 + jL_1\omega & 0 \\ 0 & R_2 + jL_2\omega \end{bmatrix} \tag{7}$$

with $Y_{j12} = -jC_F\omega$.

The last step of parameter's extraction is to obtain the bias-dependent elements of the intrinsic impedance matrix $[Z]_i$. Thus, one has

$$[Y]_i = [Y]_j - \begin{bmatrix} -jC_F\omega & jC_F\omega \\ jC_F\omega & -jC_F\omega \end{bmatrix}. \tag{8}$$

Then, one transforms the $[Y]_i$ matrix into its impedance representation $[Z]_i$ and deduces the following successively:

- the intrinsic base resistance:

$$R_B = \mathrm{Re}\,[Z_{11} - Z_{12}]_i; \tag{9}$$

- the intrinsic emitter–base resistance:

$$Z_{12i} = R_0 + \frac{R_E}{R_E^2 C_E^2\omega^2 + 1} - j\frac{R_E^2 C_E\omega}{R_E^2 C_E^2\omega^2 + 1} \tag{10}$$

  where $\omega \to 0$, one has $\mathrm{Re}\,[Z_{12i}] \to R_0 + R_E$;
- the intrinsic emitter–base capacitance:
  where $\omega \to \infty$, one has $1/(\mathrm{Im}\,[Z_{12i}] \cdot \omega) \to C_E$;

TABLE I
EXTRACTED ELEMENTS OF THE SMALL SIGNAL EQUIVALENT CIRCUIT AT DIFFERENT BIAS CONDITIONS, FOR AN EMITTER EFFECTIVE AREA OF $3 \times 20\ \mu\mathrm{m}^2$

I_c (mA)	I_b (mA)	R_1 (Ω)	L_1 (pH)	R_B (Ω)	C_F (fF)	R_2 (Ω)	L_2 (pH)	C_E (pF)	R_Q (KΩ)	C_Q (fF)	α	τ (ps)	R_0 (Ω)	R_E (Ω)
0	0	4.38	86.5			1.6	11.7							
1	0.034			6.72	59.1			1.66	36	160	0.930	8.79	2.9	38.2
2	0.062			5.17				2.94	23	158	0.948	6.22		21.2
4	0.109			4.29				5.35	12	148	0.970	4.72		9.7
6	0.151			3.2				7.32	11	130	0.973	3.89		7.5
8	0.191			2.7				9.3	10.5	143	0.975	3.62		5.5
10	0.230			2.44				11.2	11	139	0.980	3.28		4.6

TABLE II
EXTRACTED ELEMENTS OF THE SMALL SIGNAL EQUIVALENT CIRCUIT AT DIFFERENT BIAS CONDITIONS, FOR AN EMITTER EFFECTIVE AREA OF $3 \times 12\ \mu\mathrm{m}^2$

I_c(mA)	I_b(mA)	R_1 (Ω)	L_1 (pH)	R_B (Ω)	C_F (fF)	R_2 (Ω)	L_2 (pH)	C_E (pF)	R_Q (KΩ)	C_Q (fF)	α	τ (ps)	R_0 (Ω)	R_E (Ω)
0		4.1	57.9			2.45	28.8							
1	0.029			14.8	35			1.54	28	110	0.946	6.87	5.2	35
2	0.050			12				2.9	15	98	0.972	5.1		15.2
4	0.084			8.9				4.9	12	89	0.984	3.86		7.4
6	0.113			7.5				6.3	9	80	0.985	3.27		5.6
8	0.140			6.6				7.8	11.2	75	0.982	2.92		4.2
10	0.166			5.9				10.1	10.5	75	0.972	2.70		2.8

- the intrinsic base–collector capacitance:

$$Z_{22i} - Z_{21i} = \frac{R_Q}{R_Q^2 C_Q^2\omega^2 + 1} - j\frac{R_Q^2 C_Q\omega}{R_Q^2 C_Q^2\omega^2 + 1} \tag{11}$$

  where $\omega \to \infty$, one has $1/(\mathrm{Im}\,[Z_{22} - Z_{21}]_i \cdot \omega) = C_Q$;
- the intrinsic base–collector resistance:
  where $\omega \to 0$, one has $\mathrm{Re}\,[Z_{22} - Z_{21}]_i = R_Q$;
- the base transport coefficient:

$$\begin{aligned} \alpha &= \alpha_0 e^{-j\omega\tau} \\ &= \alpha_0(\cos\,\omega\tau - j\,\sin\,\omega\tau) \\ &= \frac{Z_{12i} - Z_{21i}}{Z_{22i} - Z_{21i}} \end{aligned} \tag{12}$$

  with

$$\alpha_0 = \sqrt{\left|\frac{Z_{12i} - Z_{21i}}{Z_{22i} - Z_{21i}}\right|}$$

  and

$$\tau = -\left(\frac{1}{\omega}\right)\left\{a\,\tan\left(\frac{\mathrm{Im}\,[Z_{12i} - Z_{21i}]}{\mathrm{Re}\,[Z_{12i} - Z_{21i}]}\right) - a\,\tan\left(\frac{\mathrm{Im}\,[Z_{22i} - Z_{21i}]}{\mathrm{Re}\,[Z_{22i} - Z_{21i}]}\right)\right\}.$$

Finally, to calculate R_0, which is bias independent, one plots $R_0 + R_E$ as a function of the inverse of the emitter current (I_e^{-1}). The element R_0 is then deduced from extrapolation at the origin

$$R_0 + R_E = R_0 + \frac{\eta KT}{qI_e}. \tag{13}$$

η is the ideality factor of the emitter which is found about 1.1 for these devices.

Tables I and II give the different extracted elements at different bias points.

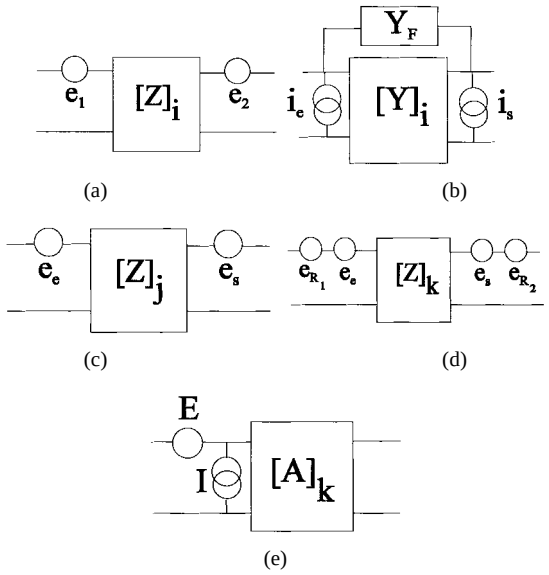

Fig. 2. (a) Intrinsic impedance representation with the input and output associated voltage noise sources e_1 and e_2, respectively. (b) Intrinsic admittance representation by adding the feedback capacitance C_F with the input and output associated current noise sources i_e and i_s, respectively. (c) Transformation of the (b) configuration in its impedance representation. (d) Influence of the parasitic access base and collector resistances with their associated thermal voltage noise generators E_{R1} and E_{R2}, respectively. (e) Chain representation of the extrinsic device with its input associated current and voltage noise sources.

III. Noise Calculations

It is now possible to make a new equivalent circuit including the different noise sources which have physical significance (Fig. 1). A thermal noise source is attributed to the intrinsic base resistance and to R_0. Furthermore, the model contains two independent shot noise sources which are both totally uncorrelated. The former is a noise voltage generator e_{R_E} in series with the dynamic emitter resistance R_E, and the latter is a noise current generator i_{cp} in parallel to the collector junction.

The intrinsic part of the device can now be transformed in a noiseless network with two noise voltage sources e_1 and e_2 [see Fig. 2(a)]. The following expressions are obtained:

$$\overline{e_1^2} = \overline{e_{R_0}^2} + \overline{e_{R_B}^2} + |Z_E|^2 \frac{\overline{e_{R_E}^2}}{R_E^2} \tag{14}$$

$$\overline{e_2^2} = \overline{e_{R_0}^2} + |Z_E|^2 \overline{i_{R_E}^2} + |Z_Q|^2 \overline{i_{cp}^2} \tag{15}$$

$$\overline{e_1 e_2^*} = \overline{e_{R_0}^2} + |Z_E|^2 \overline{i_{R_E}^2} \tag{16}$$

$$\overline{e_2 e_1^*} = \overline{e_1 e_2^*} \tag{17}$$

with $\overline{e_{R_0}^2} = 4KTR_0\Delta f$, $\overline{e_{R_B}^2} = 4KTR_B\Delta f$, $\overline{e_{R_e}^2} = 2KTR_E\Delta f$, and $\overline{i_{cp}^2} = [2KT(\alpha_0 - |\alpha|^2)/R_E]\Delta f$ [6], Z_E and Z_Q are the impedance of the emitter–base and base–collector junctions, respectively.

Then, the network is transformed in its admittance representation to which the feedback capacitance C_F is added [see Fig. 2(b)]. Both current generators and the resultant admittance matrix are expressed as follows:

$$\overline{i_e^2} = \overline{e_1^2}|Y_{11}|^2 + 2\,\mathrm{Re}\,[Y_{11}Y_{12}^*\overline{e_1 e_2^*}] + |Y_{12}|^2\overline{e_2^2} \tag{18}$$

$$\overline{i_s^2} = \overline{e_1^2}|Y_{21}|^2 + 2\,\mathrm{Re}\,[Y_{21}Y_{22}^*\overline{e_1 e_2^*}] + |Y_{22}|^2\overline{e_2^2} \tag{19}$$

$$\overline{i_e i_s^*} = Y_{21}^*Y_{11}\overline{e_1^2} + Y_{22}^*Y_{11}\overline{e_1 e_2^*} + Y_{12}Y_{21}^*\overline{e_2 e_1^*} + Y_{22}^*Y_{12}\overline{e_2^2} \tag{20}$$

$$\overline{i_s i_e^*} = Y_{11}^*Y_{21}\overline{e_1^2} + Y_{11}^*Y_{22}\overline{e_2 e_1^*} + Y_{21}Y_{12}^*\overline{e_1 e_2^*} + Y_{12}^*Y_{22}\overline{e_2^2}. \tag{21}$$

The above-considered Y_{ij}-parameters belong to the $[Y]_i$ matrix

$$\begin{bmatrix} Y_{11} & Y_{12} \\ Y_{21} & Y_{22} \end{bmatrix}_i + \begin{bmatrix} Y_F & -Y_F \\ -Y_F & Y_F \end{bmatrix} = [Y]_j. \tag{22}$$

The $[Y]_j$ matrix is transformed into the $[Z]_j$ impedance representation with its two series noise voltage generators e_e and e_s [see Fig. 2(c)], in order to add the parasitic series access elements with

$$\overline{e_e^2} = \overline{i_e^2}|Z_{11}|^2 + 2\,\mathrm{Re}\,[Z_{11}Z_{12}^*\overline{i_e i_s^*}] + |Z_{12}|^2\overline{i_s^2} \tag{23}$$

$$\overline{e_s^2} = \overline{i_e^2}|Z_{21}|^2 + 2\,\mathrm{Re}\,[Z_{21}Z_{22}^*\overline{i_e i_s^*}] + |Z_{22}|^2\overline{i_s^2} \tag{24}$$

$$\overline{e_e e_s^*} = Z_{21}^*Z_{11}\overline{i_e^2} + Z_{22}^*Z_{11}\overline{i_e i_s^*} + Z_{12}Z_{21}^*\overline{i_s i_e^*} + Z_{22}^*Z_{12}\overline{i_s^2} \tag{25}$$

$$\overline{e_s e_e^*} = Z_{11}^*Z_{21}\overline{i_e^2} + Z_{11}^*Z_{22}\overline{i_s i_e^*} + Z_{21}Z_{12}^*\overline{i_e i_s^*} + Z_{12}^*Z_{22}\overline{i_s^2}. \tag{26}$$

The above-considered Z_{ij} parameters belong to the $[Z]_j$ matrix.

The final step of the noise calculations is to obtain the noise of the total extrinsic transistor. Therefore, the $[Z]_j$ matrix is transformed into the impedance matrix $[Z]_k$ and one deduces the two terminal series noise voltage generators E_1 and E_2 by adding the noise voltage sources e_{R_1} and e_{R_2} associated with R_1 and R_2, respectively [see Fig. 2(d)],

$$\begin{bmatrix} Z_{11} & Z_{12} \\ Z_{21} & Z_{22} \end{bmatrix}_j + \begin{bmatrix} R_1 + jL_1\omega & 0 \\ 0 & R_2 + jL_2\omega \end{bmatrix} = [Z]_k \tag{27}$$

where

$$\overline{E_1^2} = \overline{e_e^2} + \overline{e_{R_1}^2} \tag{28}$$

$$\overline{E_2^2} = \overline{e_s^2} + \overline{e_{R_2}^2} \tag{29}$$

$$\overline{E_1 E_2^*} = \overline{e_e e_s^*} \tag{30}$$

$$\overline{E_2 E_1^*} = \overline{e_s e_e^*} \tag{31}$$

with $\overline{e_{R_1}^2} = 4KTR_1\Delta f$ and $\overline{e_{R_2}^2} = 4KTR_2\Delta f$.

Nevertheless, in order to obtain the noise parameters directly, it is necessary to display the extrinsic network in its chain representation [see Fig. 2(e)]. $[Z]_k$ is transformed into the chain matrix $[A]_k$ and one obtains the final expressions

$$\overline{E^2} = \overline{E_1^2} - 2\,\mathrm{Re}\,[A_{11}\overline{E_1^* E_2}] + |A_{11}|^2\overline{E_2^2} \tag{32}$$

$$\overline{I^2} = |A_{21}|^2\overline{E_2^2} \tag{33}$$

$$\overline{EI^*} = -A_{21}^*\overline{E_1 E_2^*} + A_{11}A_{21}^*\overline{E_2^2} \tag{34}$$

$$\overline{IE^*} = -A_{21}\overline{E_2 E_1^*} + A_{21}A_{11}^*\overline{E_2^2}. \tag{35}$$

$$\Re_1 = R_1 + \frac{R_B(1 - R_BC_FR_QC_Q\omega^2) + R_BR_QC_Q(R_QC_Q + R_QC_F + R_BC_F)\omega^2}{(1 - R_BC_FR_QC_Q\omega^2)^2 + (R_QC_Q + R_QC_F + R_BC_F)^2\omega^2} \tag{3}$$

$$\Im_1 = L_1\omega + \frac{R_BR_QC_Q\omega(1 - R_BC_FR_QC_Q\omega^2) - R_B(R_QC_Q + R_QC_F + R_BC_F)\omega}{(1 - R_BC_FR_QC_Q\omega^2)^2 + (R_QC_Q + R_QC_F + R_BC_F)^2\omega^2} \tag{4}$$

$$\Re_2 = R_2 + \frac{R_Q(1 - R_BC_FR_QC_Q\omega^2)}{(1 - R_BC_FR_QC_Q\omega^2)^2 + (R_QC_Q + R_QC_F + R_BC_F)^2\omega^2} \tag{5}$$

$$\Im_2 = L_2\omega + \frac{-R_Q(R_QC_Q + R_QC_F + R_BC_F)\omega}{(1 - R_BC_FR_QC_Q\omega^2)^2 + (R_QC_Q + R_QC_F + R_BC_F)^2\omega^2} \tag{6}$$

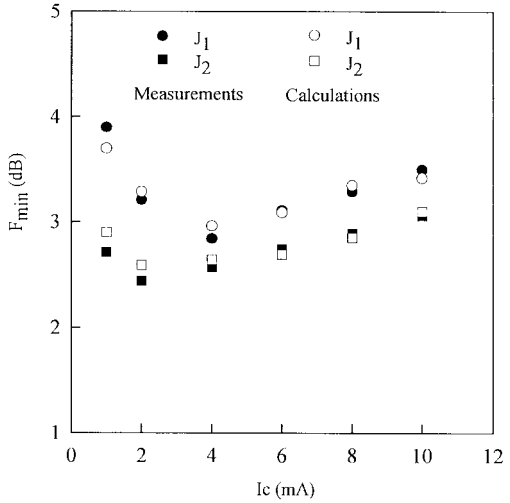

Fig. 3. Comparisons between calculated and measured minimum noise figure $F_{\min}$ versus collector current I_c at frequency $f = 10$ GHz, for two different geometries $Ae = 3 \times 12\ \mu\text{m}^2$ (J_1) and $Ae = 3 \times 20\ \mu\text{m}^2$ (J_2).

The four noise parameters are derived from

$$C_{A_k} = \frac{1}{2\Delta f}\begin{bmatrix} \overline{E^2} & \overline{EI^*} \\ \overline{E^*I} & \overline{I^2} \end{bmatrix} = 2KT\begin{bmatrix} R_n & \dfrac{N_{F_{\min}}-1}{2} - R_n Y_{\text{opt}}^* \\ \dfrac{N_{F_{\min}}-1}{2} - R_n Y_{\text{opt}} & R_n|Y_{\text{opt}}|^2 \end{bmatrix} \tag{36}$$

with

$$N_{F_{\min}} = 1 + \frac{1}{2KT\Delta f}\left\{\text{Re}\,[\overline{EI^*}] + \sqrt{\overline{E^2}\,\overline{I^2} - [\text{Im}\,(\overline{EI^*})^2]}\right\}$$

$$R_n = \frac{\overline{E^2}}{4KT\Delta f}$$

$$G_{\text{opt}} = \sqrt{\frac{\overline{I^2}}{\overline{E^2}} - \left[\frac{\text{Im}\,(\overline{EI^*})}{\overline{E^2}}\right]^2}$$

and

$$B_{\text{opt}} = \frac{\text{Im}\,(\overline{EI^*})}{\overline{E^2}}.$$

R_n is the equivalent noise resistance of the device, G_{opt} and B_{opt} [7] are the real and imaginary parts of the optimum input admittance to obtain the minimum noise figure.

IV. RF Noise Performances

The noise figure measurements were performed using an HP8970B noise figure meter. The test set included a coaxial single slug input tuner for measuring the minimum noise figure ($F_{\min}$).

Fig. 3 compares noise calculations and measurements of $F_{\min}$ as a function of the collector current at $V_{ce} = 1.5$ V and $f = 10$ GHz. One notices that the method previously developed allows the minimum of $F_{\min}$ to be located with good precision. One obtains an $F_{\min}$ of about 2.5 dB at $I_c = 2.8$ mA (J_2) and $I_c = 4$ mA (J_1). The decrease of $F_{\min}$ in the collector current range from 0 to 3 mA is due to the slight decrease of R_B as the collector current increases. This implies that its associated thermal noise also diminishes. On the other hand, the positive slope of $F_{\min}$ ($I_c = 3$ to 10 mA) is related to the increasing contribution of the shot noise. In fact, the dynamic emitter–base resistance is inversely proportional to the emitter current and, as a consequence, it affects the term $\overline{i_{R_e}^2}$.

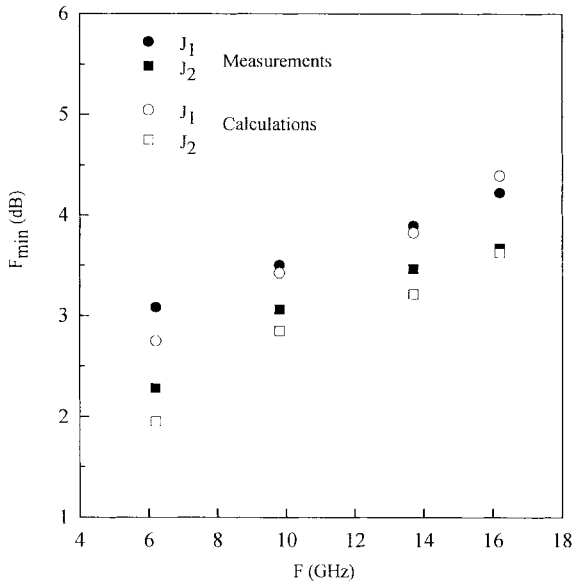

Fig. 4. Comparisons between calculated and measured minimum noise figure $F_{\min}$ versus frequency at a collector current $Ic = 10$ mA, for two different geometries $Ae = 3 \times 12\ \mu\text{m}^2$ (J_1) and $Ae = 3 \times 20\ \mu\text{m}^2$ (J_2).

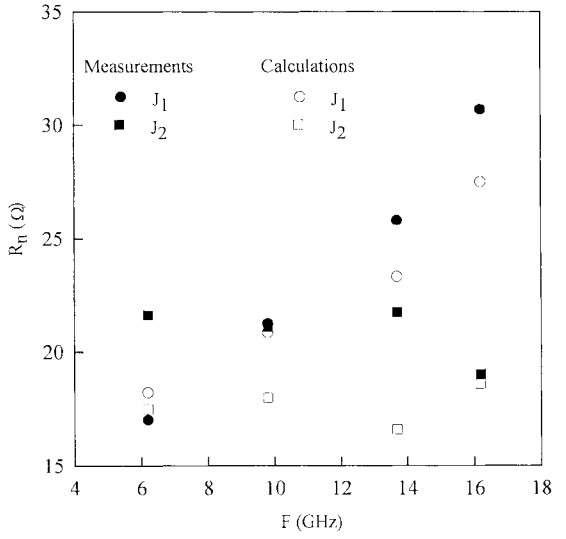

Fig. 5. Comparisons between calculated and measured equivalent noise resistance R_n versus frequency at a collector current $I_c = 10$ mA, for two different geometries $A_e = 3 \times 12\ \mu\text{m}^2$ (J_1) and $A_e = 3 \times 20\ \mu\text{m}^2$ (J_2).

Fig. 4 shows $F_{\min}$ as a function of frequency at a nominal bias fixed by the constructor ($I_c = 10$ mA). The noise figure approaches a linear law. The agreement is 0.3 dB over the whole frequency range. This can be attributed to the fact that $F_{\min}$ is very sensitive to the emitter and base resistances, thus it depends on the accuracy of the parameters extraction.

Fig. 5 presents the equivalent noise resistance R_n. A good agreement is observed between measurements and the modelization, even if R_n seems to be the most difficult parameter to obtain because of the uncertainty of S-parameter measurements.

Figs. 6 and 7 display the optimum input impedance magnitude and phase, respectively, which are both linear as a function of frequency.

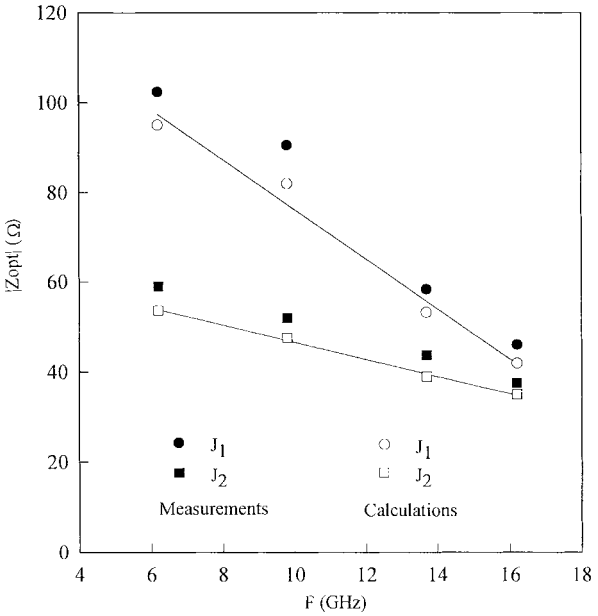

Fig. 6. Comparisons between calculated and measured optimum input impedance magnitude versus frequency at a collector current $I_c = 10$ mA, for two different geometries $A_e = 3 \times 12\ \mu\text{m}^2$ (J_1) and $A_e = 3 \times 20\ \mu\text{m}^2$ (J_2).

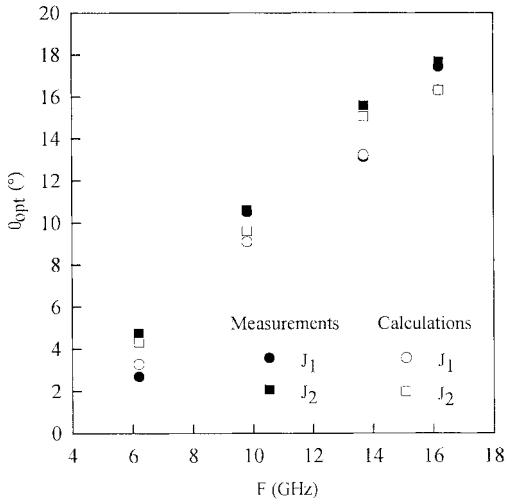

Fig. 7. Comparisons between calculated and measured optimum input impedance phase versus frequency at a collector current $I_c = 10$ mA, for two different geometries $A_e = 3 \times 12\ \mu\text{m}^2$ (J_1) and $A_e = 3 \times 20\ \mu\text{m}^2$ (J_2).

V. Conclusion

By means of a simple application of the circuit theory of linear noisy networks it has been demonstrated that this method can be applied to relatively complex circuits.Furthermore, it has been shown that the noise parameters can be easily calculated and are in good agreement with noise measurements. This method presents the advantage that all parasitic effects of the model are taken into account. In order to summarize the results, the origin of the noise in HBT's structures seems to be related to the intrinsic base resistance at low collector currents and to the shot noise linked with the dynamic emitter–base resistance as the current increases. Microelectronic engineers could take easy advantage of this method because it permits the prediction with good precision of the noise of complex structures only by means of S-parameter measurements, avoiding the noise measurements which are quite difficult to perform.

Acknowledgment

The authors wish to thank GEC Marconi for providing the devices cited in this paper.

References

[1] S. Lee and A. Gopinath, "Parameter extraction technique for HBT equivalent circuit using cutoff mode measurement," *IEEE Trans. Electron Devices*, vol. 40, pp. 574–577, Mar. 1992.

[2] D. Costa, W. Liu, and J. Harris, "Direct extraction of the AlGaAs/GaAs heterojunction bipolar transistor small-signal equivalent circuit," *IEEE Trans. Electron Devices*, vol. 38, pp. 2018–2024, Sept. 1991.

[3] J. S. Park and A. Neugroschel, "Parameter extraction for bipolar transistors," *IEEE Trans. Electron Devices*, vol. 36, pp. 88–95, Aug. 1989.

[4] U. Shaper, "Analytical parameter extraction of the HBT equivalent circuit with T-like topology from measured S-parameters," *IEEE Trans. Microwave Theory Tech.*, vol. 43, pp. 493–498, Mar. 1995.

[5] H. Hillbrand and P. H. Russer, "An efficient method for computer aided noise analysis of linear amplifier networks," *IEEE Trans. Circuits Syst.* vol. CAS-23, pp. 235–238, Apr. 1976.

[6] R. J. Hawkins, "Limitations of Nielsen's and related noise equations applied to microwave bipolar transistors, and a new expression for the frequency and current dependent noise figure," *Solid State Electron.*, vol. 20, pp. 191–196, July 1977.

[7] D. Gasquet and F. Barberousse, "Determination of PHEMT's microwave noise parameters only by means of the small-signal equivalent circuit and experimental comparisons," *J. Phys. III*, vol. 5, pp. 495–507, May 1995.